

# High stability of faceted nanotubes and fullerenes of multi-phase layered phosphorus: A computational study

Jie Guan, Zhen Zhu, and David Tománek\*

*Physics and Astronomy Department, Michigan State University, East Lansing, Michigan 48824, USA*

(Dated: November 6, 2014)

We present a paradigm in constructing very stable, faceted nanotube and fullerene structures by laterally joining nanoribbons or patches of different planar phosphorene phases. Our *ab initio* density functional calculations indicate that these phases may form very stable, non-planar joints. Unlike fullerenes and nanotubes obtained by deforming a single-phase planar monolayer at substantial energy penalty, we find faceted fullerenes and nanotubes to be nearly as stable as the planar single-phase monolayers. The resulting rich variety of polymorphs allows to tune the electronic properties of phosphorene nanotubes (PNTs) and fullerenes not only by the chiral index, but also by the combination of different phosphorene phases. In selected PNTs, a metal-insulator transition may be induced by strain or changing the number of walls.

PACS numbers: 61.46.-w, 61.48.De, 71.20.Tx, 73.22.-f

One reason for the unprecedented interest in graphitic carbon is its ability to form not only self-supporting graphene layers [1, 2], but also single- and multi-wall nanotubes [3] and fullerenes [4]. Similar to graphite, which is the parent compound of these carbon allotropes, the stable black phosphorus allotrope is a layered compound that can be exfoliated to phosphorene monolayers [5, 6]. Phosphorus nanotubes [7, 8] and fullerenes [9–11] have been postulated to form in analogy to their carbon counterparts by deforming a phosphorene monolayer, typically at significant energy cost. In contrast to the unique structure of planar graphene, at least four equally stable phases with different properties,  $\alpha$ -P,  $\beta$ -P,  $\gamma$ -P and  $\delta$ -P, can be distinguished in the puckered structure of a phosphorene monolayer [12–14]. The ability of the different phases to form non-planar in-layer connections at essentially zero energy cost suggests the possibility to form faceted nanotube and fullerene structures that are as stable as planar phosphorene. The possibility to mix different phases within each wall of spherical and cylindrical single- and multi-wall structures would offer unprecedented richness not only of form, but also the associated electronic properties. Bulk quantities of carbon nanotubes and fibers are currently used as a performance-enhancing additive to graphite in Li-ion batteries (LIBs) [15]. Since black phosphorus is considered superior to graphite for LIB applications [16, 17], a similar benefit could be derived from the presence of phosphorene nanotubes and related structures.

Here we present a new paradigm in constructing very stable, faceted nanotube and fullerene structures by laterally joining nanoribbons or patches of different planar phosphorene phases. Our *ab initio* density functional calculations indicate that these phases may connect laterally at an angle. Unlike fullerenes and nanotubes obtained by deforming a single-phase planar monolayer at substantial energy penalty, we find faceted fullerenes and nanotubes to be nearly as stable as planar single-phase monolayers.

The resulting rich variety of polymorphs allows to tune the electronic properties of phosphorene nanotubes and fullerenes not only by the chiral index, but also by the combination of different phosphorene phases. In selected PNTs, a metal-insulator transition may be induced by strain or by changing the number of walls.

We utilize *ab initio* density functional theory (DFT) as implemented in the SIESTA [18] code to obtain insight into the equilibrium structure, stability and electronic properties of nanotubes and fullerenes based on different layered phosphorus allotropes. We use periodic boundary conditions throughout the study, with nanotubes and fullerenes separated by a vacuum region exceeding 15 Å. We utilize the Perdew-Burke-Ernzerhof (PBE) [19] exchange-correlation functional, norm-conserving Troullier-Martins pseudopotentials [20], and a double- $\zeta$  basis including polarization orbitals. Van der Waals interactions are described using the OptB86b-vdW functional [21, 22] as implemented in the VASP [23] code. We sample the reciprocal space by a fine grid [24] of 8  $k$ -points for 1D Brillouin zone of nanotubes and only 1  $k$ -point for the small Brillouin zone of isolated fullerenes. We use a mesh cutoff energy of 180 Ry to determine the self-consistent charge density, which provides us with a precision in total energy of  $\lesssim 2$  meV/atom. We discuss geometries that have been optimized using the conjugate gradient method [25] until none of the residual Hellmann-Feynman forces exceeded  $10^{-2}$  eV/Å.

The nanotube and fullerene structures presented in this study are formed by laterally connecting the different stable allotropes of layered phosphorus, namely  $\alpha$ -,  $\beta$ -,  $\gamma$ - and  $\delta$ -P, which are shown in Fig. 1(a). Whereas  $\alpha$ - and  $\beta$ -P are the most stable allotropes with  $E_{coh} = 3.28$  eV/atom in the monolayer, the stability of  $\gamma$ - and  $\delta$ -P is lower only by  $< 0.1$  eV/atom [13]. All these structures share the underlying honeycomb lattice with graphene, but – in contrast to graphene – are not flat. In analogy to graphene, we define the armchair and zigzag

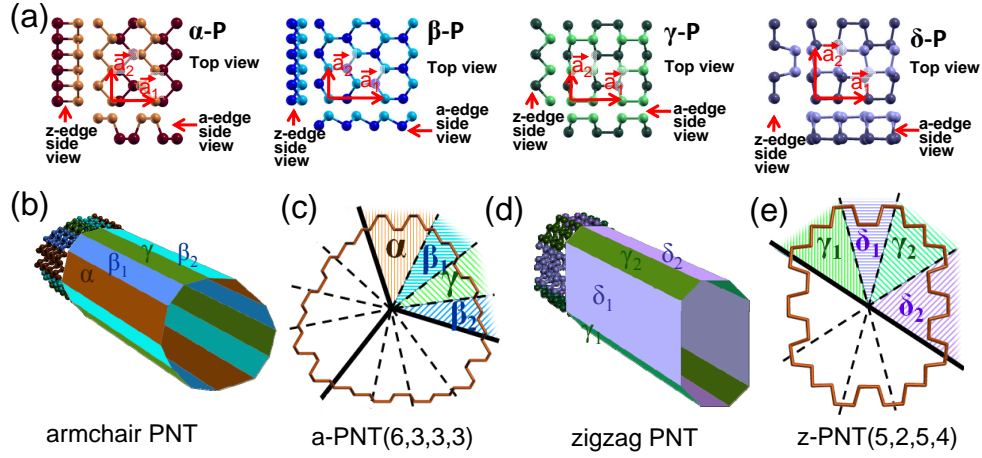


FIG. 1. (Color online) (a) Atomic structure of  $\alpha$ -,  $\beta$ -,  $\gamma$ - and  $\delta$ -P in top view and the side view of zigzag and armchair edges. The orthogonal lattice vectors  $\vec{a}_1$  and  $\vec{a}_2$  define the unit cells or supercells used in this study. Schematic and atomic structure of (b) an armchair and (d) a zigzag PNT, with the different structural phases distinguished by color and shading. The cross-sections of (c) an armchair and (e) a zigzag nanotube illustrate the symmetry and the distribution of phases along the perimeter.

edges of the different phosphorene phases in Fig. 1(a). The vectors  $\vec{a}_1$  and  $\vec{a}_2$ , which span these lattices, may also be used to identify the edges of phosphorene nanoribbons (PNRs). Considering the equilibrium non-planar connections between  $\alpha$ -,  $\beta$ -,  $\gamma$ -P along zigzag edges and  $\gamma$ -,  $\delta$ -P along armchair edges [13], we can design two types of faceted nanotubes.

The exact morphology of the more common carbon nanotubes (CNTs) is defined by the chiral index  $(n_1, n_2)$ , which is associated with the chiral vector  $\vec{C}_h = n_1\vec{a}_1 + n_2\vec{a}_2$  on a graphene monolayer. This vector defines the wrapping into a nanotube and identifies its edge. There is a common distinction between armchair nanotubes (a-NTs) with an armchair edge and zigzag nanotubes (z-NTs) with a zigzag edge. A similar convention could be used when bending monolayers of  $\alpha$ -,  $\beta$ -,  $\gamma$ - and  $\delta$ -P to corresponding nanotubes.

The nanotubes we consider here are very different, as they are formed by connecting planar narrow nanoribbons of different phosphorene allotropes. Armchair nanotubes (a-PNTs), shown in Fig. 1(b) and 1(c), form by connecting laterally  $\alpha$ -PNRs with  $\beta$ - and  $\gamma$ -PNRs along their zigzag edges. Virtually no deformation is required to form a nanotube with  $C_3$  symmetry and a polygonal cross-section, shown in Fig. 1(c). The three identical  $120^\circ$  segments in the cross-section of this a-PNT contain, in this sequence, an  $\alpha$ -PNR connected to a  $\beta$ -PNR,  $\gamma$ -PNR, and  $\beta$ -PNR. The width of each individual PNR may be zero or nonzero, giving rise to many different morphologies, illustrated in the Supplemental Material [26]. Since the two  $\beta$ -PNRs in this segment may also have a different width, we distinguish them by the subscript. Next, we imagine joining laterally all nanoribbons of a given phase  $\epsilon$  to a wider ribbon of width  $W_\epsilon = n_\epsilon|\vec{a}_1|$ . Obtaining in this way the values  $n_\alpha$ ,  $n_{\beta_1}$ ,  $n_\gamma$  and  $n_{\beta_2}$ , we may char-

acterize an armchair nanotube as a-PNT( $n_\alpha, n_{\beta_1}, n_\gamma, n_{\beta_2}$ ) and identify the nanotube in Fig. 1(c) as a-PNT(6,3,3,3).

In analogy to a-PNTs, zigzag nanotubes (z-PNTs), shown in Fig. 1(d) and 1(e), form by connecting laterally  $\gamma$ - and  $\delta$ -PNRs along their armchair edges. Virtually no deformation is required to form a nanotube with  $C_2$  symmetry and a polygonal cross-section, shown in Fig. 1(e). The two identical  $180^\circ$  segments in the cross-section of this z-PNT contain, in this sequence, a  $\gamma$ -PNR connected to a  $\delta$ -PNR,  $\gamma$ -PNR, and  $\delta$ -PNR. The width of each individual PNR may be zero or nonzero, giving rise to many different morphologies, also illustrated in the Supplemental Material [26]. Since the two  $\gamma$ - and the two  $\delta$ -PNRs in this segment may also have a different width, we distinguish them by the subscript. Next, we imagine joining laterally all nanoribbons of the same phase  $\epsilon$  to a wider ribbon of width  $W_\epsilon = n_\epsilon|\vec{a}_2|$ . Obtaining in this way the values  $n_{\gamma_1}$ ,  $n_{\delta_1}$ ,  $n_{\gamma_2}$  and  $n_{\delta_2}$ , we may characterize a zigzag nanotube as z-PNT( $n_{\gamma_1}, n_{\delta_1}, n_{\gamma_2}, n_{\delta_2}$ ) and identify the nanotube in Fig. 1(e) as z-PNT(5,2,5,4). We do not discuss here the narrowest z-PNT(1,0,1,0) with a  $P_4$  square in the cross-section, which is in reality a nanowire.

Whereas the designation a-PNT( $n_\alpha, n_{\beta_1}, n_\gamma, n_{\beta_2}$ ) defines the way to construct a unique armchair nanotube from PNRs, a given nanotube may be characterized by different sets of chiral indices. As discussed in the Supplemental Material [26], this ambiguity stems from the arbitrariness in assigning atoms at a nanoribbon connection to either side and can be avoided by selecting  $n_\alpha = \max$ . A similar ambiguity in the nomenclature of z-PNTs can be avoided by selecting  $n_{\gamma_1} = \max$  and  $n_{\gamma_2} = \max$ .

Similar to the construction of nanotubes by connecting nanoribbons of different phases, also fullerenes may be constructed by connecting planar triangular segments of  $\beta$ -P monolayers by narrow  $\gamma$ -P strips at the

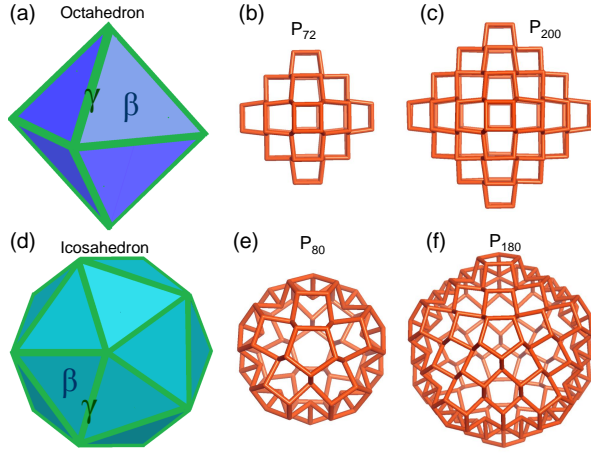


FIG. 2. (Color online) Phosphorene-based fullerene structures with (a-c) octahedral and (d-f) icosahedral symmetry. The structural models in (a) and (d) indicate, how triangular facets of  $\beta$ -P are connected by  $\gamma$ -P along the edges. The stick models of  $P_{72}$  in (b),  $P_{200}$  in (c),  $P_{80}$  in (e) and  $P_{180}$  in (f) depict the relaxed atomic structures of octahedral and icosahedral fullerenes.

edges, as shown in Fig. 2. We have considered octahedral fullerenes, illustrated schematically in Fig. 2(a), and icosahedral fullerenes, illustrated schematically in Fig. 2(d). Ideal  $P_n$  octahedral fullerenes contain  $n = 8m^2$  atoms and icosahedral fullerenes contain  $n = 20m^2$  atoms, where  $m$  is an integer. Two examples of octahedral fullerenes are presented in Figs. 2(b) and 2(c), and two examples of icosahedral fullerenes in Figs. 2(e) and 2(f). Since these structures do not require significant deformation of the planar monolayer structure, but rather results from an optimum connection between  $\beta$ -P and  $\gamma$ -P, they also are expected to be nearly as stable as the planar single-phase allotropes.

Our results for the relative stability of phosphorene nanotubes are presented in Fig. 3(a) and those for fullerenes in Fig. 3(b). In both sub-figures, the dashed lines display the expected  $1/R^2$  behavior of the strain energy per atom  $\Delta E/n$  on the radius  $R$  that energetically penalizes structures with small radii.

As seen in Fig. 3(a), this projected behavior, based on continuum elasticity theory [27], agrees closely with our results for pure  $\beta$ - and  $\gamma$ -P nanotubes and previously published results for  $\beta$ -P nanotubes, based on density functional based tight-binding (DFTB) calculations [8]. As anticipated originally, the faceted multi-component nanotubes are much more stable than these. We find that (i) their strain energies are nearly independent of the radius and (ii) their relative stabilities lie in the value range delimited by the stabilities of the pure planar components, indicated by the shaded region. Since z-PNTs contain the least stable  $\gamma$  and  $\delta$  phases, they are also least stable among the faceted nanotubes. Presence of the most stable  $\alpha$  and  $\beta$  phases, on the other hand, makes

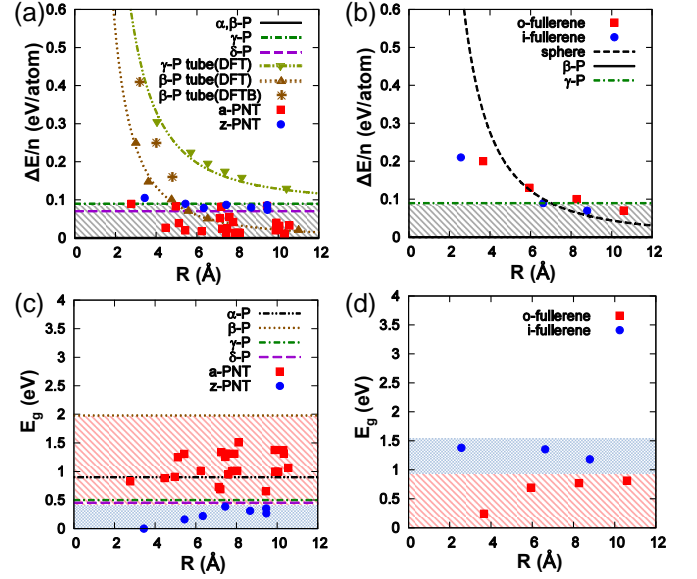


FIG. 3. (Color online) Stability and electronic structure of faceted nanotubes and fullerenes. (a) Average strain energy per atom  $\Delta E/n$  in PNTs of different radius  $R$  with respect to a planar  $\beta$ -P monolayer. The shaded region indicates the range of stabilities of different planar phases and contains most data points for multi-component faceted nanotubes. For the sake of comparison, we also present data points for pure-phase PNTs obtained by rolling up  $\beta$ - and  $\gamma$ -P to a tube. (b) Strain energy per atom in octahedral (o) and icosahedral (i) fullerenes of radius  $R$ . The dashed lines in (a) and (b) represent the  $1/R^2$  behavior based on continuum elasticity theory for pure-phase nanostructures. (c) Fundamental band gaps  $E_g$  in faceted a-PNTs and z-PNTs. The horizontal lines depict  $E_g$  values in pure planar phosphorene monolayers and help to rationalize the separation between large gap values in a-PNTs and small gap values in z-PNTs. (d) HOMO-LUMO gaps in o- and i-fullerenes. O-fullerenes have consistently larger band gaps than i-fullerenes.

a-PNTs consistently more stable than z-PNTs.

Stability enhancement caused by the coexistence of multiple phases can also be observed in our results for fullerenes in Fig. 3(b). As in the nanotubes, we find most strain energies within the value range delimited by the pure planar  $\beta$ - and  $\gamma$ -P phases. The stability enhancement is best visible in very small fullerenes. Interestingly, we find the small fullerene structures more stable than  $P_4$ , the building block of the (most reactive) bulk phosphorus allotrope. Our canonical molecular dynamics simulations, described in the Supplemental Material [26], show that all nanotube and fullerene structures we investigated are stable up to 1,000 K, slightly above  $T_M = 863$  K, the melting point of red phosphorus [28].

In carbon nanotubes and fullerenes, the occurrence of a fundamental band gap is a signature of quantum confinement in the underlying semi-metallic graphene structure. The advantage of phosphorene over graphene is the presence of a fundamental band gap in all layered

allotropes discussed here. We thus expect the fundamental band gaps  $E_g$  of nanotubes and fullerenes to approximately span the value range of the pure components, indicated by the shaded regions in Figs. 3(c) and 3(d). Even though additional corrections are expected due to quantum confinement and structural relaxation, such corrections are apparently not as important, since most of our data points lie in the range delimited by the pure components. At this point, we wish to point out that our electronic structure results in Figs. 3(c) and 3(d), obtained by DFT-PBE, are expected to underestimate the fundamental band gaps [5, 12].

As seen in Fig. 3(c), we find larger band gap values in armchair PNTs containing  $\alpha$ -,  $\beta$ - and  $\gamma$ -P, since each of the pure planar components has a band gap in excess of 0.5 eV in the monolayer. Since  $\gamma$ - and  $\delta$ -P have the smallest band gaps among the phosphorene allotropes, we also see the smallest band gaps in z-PNTs, which contain these two phases. In the narrow z-PNT(3,0,3,0), shown in the Supplemental Material [26], the close distance between third neighbors along the inner tube perimeter causes the band gap to close.

In finite-size fullerenes,  $E_g$  represents the gap between the highest occupied molecular orbital (HOMO) and the lowest unoccupied molecular orbital (LUMO). Our results in Fig. 3(d) suggest that the HOMO-LUMO gaps in icosahedral fullerenes are larger than in octahedral fullerenes. Even though the values are similar to those of nanotubes in Fig. 3(c), we can not easily rationalize the value range for o- and i-fullerenes, since both structures consist of the same  $\beta$ -P and  $\gamma$ -P allotropes.

As reported previously [5, 12, 13, 29, 30], the fundamental band gap in phosphorene depends sensitively on the number of layers and on in-layer strain. Our results in Fig. 4 indicate that the same behavior occurs also in PNTs. We find multi-wall PNTs to be stabilized by an inter-wall interaction of  $\lesssim 50$  meV/atom, roughly the same as in the layered compounds [31, 32]. Due to a large fraction of  $\gamma$ -P in the wall, which has been shown to undergo a metal-semiconductor transition, we investigated the (5,0,5,0)@(9,0,9,0) double-wall z-PNT, shown in Fig. 4(a). The density of states (DOS) of this double-wall PNT, shown in Fig. 4(b), indicates that the inter-wall interaction may turn two semiconducting nanotubes metallic upon being combined to a double-wall nanotube. As seen in Figs. 4(c) and 4(d) for the single-wall a-PNT(3,0,9,0), even a modest 5% stretch may turn a semiconducting nanotube containing a significant fraction of  $\gamma$ -P metallic. This low level of strain may be applied externally or induced by epitaxy, including structural changes induced in multi-wall nanotubes.

The most important implication of our claim that faceted nanotubes and fullerenes are as stable as planar phosphorene is that they should exist in nature and will be observed eventually, as was the case with boron nanostructures [33, 34]. We feel that phosphorus nanotubes

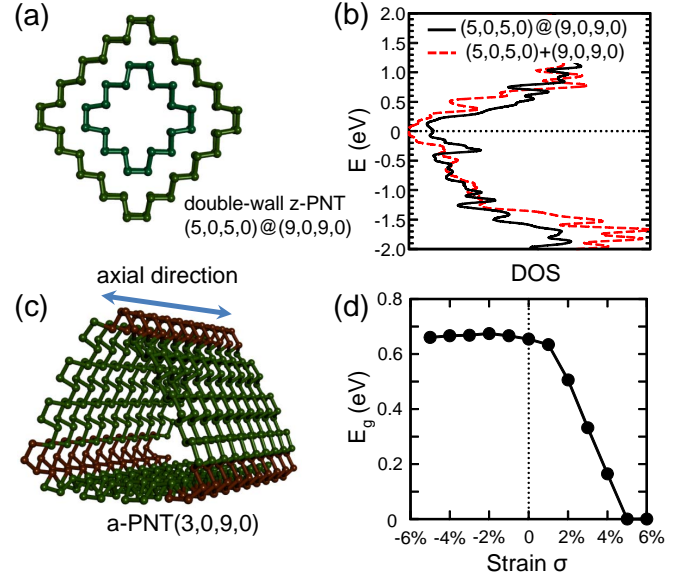


FIG. 4. (Color online) (a) Cross-section and (b) DOS of the double-wall z-PNT (5,0,5,0)@(9,0,9,0). The solid line in (b) shows the total DOS and the dashed line depicts the superposition of the densities of states of the isolated nanotube components. The Fermi level  $E_F$  is set at 0. (c) Perspective view of the a-PNT(3,0,9,0) and (d) dependence of the gap energy  $E_g$  on axial strain.

and fullerenes may form during ball milling of black phosphorus [17] under inert, oxygen-free atmosphere. This process may also produce structures with a large accessible surface area for phosphorus-based LIB applications [16, 17].

In conclusion, we have presented a new paradigm in constructing very stable, faceted nanotube and fullerene structures by laterally joining nanoribbons or patches of different planar phosphorene phases. Our *ab initio* density functional calculations indicate that these phases may form very stable, non-planar joints. Unlike fullerenes and nanotubes obtained by deforming a single-phase planar monolayer at substantial energy penalty, we find faceted fullerenes and nanotubes to be nearly as stable as the planar single-phase monolayers. The resulting rich variety of polymorphs allows to tune the electronic properties of phosphorene nanotubes and fullerenes not only by their chiral index, but also by the combination of different phosphorene phases. In selected PNTs, a metal-insulator transition may be induced by strain or changing the number of walls.

We thank Luke Shulenburg for useful discussions. This study was supported by the National Science Foundation Cooperative Agreement #EEC-0832785, titled “NSEC: Center for High-rate Nanomanufacturing”. Computational resources have been provided by the Michigan State University High Performance Computing Center.

---

\* tomanek@pa.msu.edu

- [1] K. S. Novoselov, A. K. Geim, S. V. Morozov, D. Jiang, Y. Zhang, S. V. Dubonos, I. V. Grigorieva, and A. A. Firsov, *Science* **306**, 666 (2004).
- [2] Y. Zhang, Y.-W. Tan, H. L. Stormer, and P. Kim, *Nature* **438**, 201 (2005).
- [3] S. Iijima, *Nature* **354**, 56 (1991).
- [4] H. W. Kroto, J. R. Heath, S. C. O'Brien, R. F. Curl, and R. E. Smalley, *Nature* **318**, 162 (1985).
- [5] H. Liu, A. T. Neal, Z. Zhu, Z. Luo, X. Xu, D. Tomanek, and P. D. Ye, *ACS Nano* **8**, 4033 (2014).
- [6] L. Li, Y. Yu, G. J. Ye, Q. Ge, X. Ou, H. Wu, D. Feng, X. H. Chen, and Y. Zhang, *Nature Nanotech.* **9**, 4033 (2014).
- [7] I. Cabria and J. W. Mintmire, *Europhys. Lett.* **65**, 82 (2004).
- [8] G. Seifert and E. Hernández, *Chem. Phys. Lett.* **318**, 355 (2000).
- [9] A. J. Karttunen, M. Linnolahti, and T. A. Pakkanen, *ChemPhysChem* **9**, 2550 (2008).
- [10] J.-G. Han and J. A. Morales, *Chem. Phys. Lett.* **396**, 27 (2004).
- [11] G. Seifert, T. Heine, and P. Fowler, *Europ. Phys. J. D: Atomic, Molecular, Optical and Plasma Phys.* **16**, 341 (2001).
- [12] Z. Zhu and D. Tománek, *Phys. Rev. Lett.* **112**, 176802 (2014).
- [13] J. Guan, Z. Zhu, and D. Tománek, *Phys. Rev. Lett.* **113**, 046804 (2014).
- [14] S. E. Boulfelfel, G. Seifert, Y. Grin, and S. Leoni, *Phys. Rev. B* **85**, 014110 (2012).
- [15] M. Endo, Y. Kim, T. Hayashi, K. Nishimura, T. Matsuta, K. Miyashita, and M. Dresselhaus, *Carbon* **39**, 1287 (2001).
- [16] Q. Lu, X. G. Hu, H. Chen, and Y. Z. Mao, *Chinese Patent No. ZL-03153105.9* (6 July 2005).
- [17] C.-M. Park and H.-J. Sohn, *Adv. Mat.* **19**, 2465 (2007).
- [18] E. Artacho, E. Anglada, O. Dieguez, J. D. Gale, A. Garcia, J. Junquera, R. M. Martin, P. Ordejon, J. M. Pruneda, D. Sanchez-Portal, and J. M. Soler, *J. Phys. Cond. Mat.* **20**, 064208 (2008).
- [19] J. P. Perdew, K. Burke, and M. Ernzerhof, *Phys. Rev. Lett.* **77**, 3865 (1996).
- [20] N. Troullier and J. L. Martins, *Phys. Rev. B* **43**, 1993 (1991).
- [21] J. Klimeš, D. R. Bowler, and A. Michaelides, *J. Phys.: Cond. Matt.* **22**, 022201 (2010).
- [22] J. Klimeš, D. R. Bowler, and A. Michaelides, *Phys. Rev. B* **83**, 195131 (2011).
- [23] G. Kresse and J. Furthmüller, *Phys. Rev. B* **54**, 11169 (1996).
- [24] H. J. Monkhorst and J. D. Pack, *Phys. Rev. B* **13**, 5188 (1976).
- [25] M. R. Hestenes and E. Stiefel, *J. Res. Natl. Bur. Stand.* **49**, 409 (1952).
- [26] See the Supplemental Material at <http://link.aps.org/supplemental/10.1103/PhysRevLett.000.000000> for additional information regarding nanotube nomenclature, structural and electronic properties of additional single-wall and multi-wall phosphorene nanotubes and fullerenes, molecular dynamics simulations pertaining to their thermal stability, and the effect of van der Waals interactions.
- [27] D. Tomanek, W. Zhong, and E. Krastev, *Phys. Rev. B* **48**, 15461 (1993).
- [28] C. Kittel, *Introduction to Solid State Physics*, eighth ed. (Wiley, Hoboken, NJ, 2004).
- [29] A. S. Rodin, A. Carvalho, and A. H. Castro Neto, *Phys. Rev. Lett.* **112**, 176801 (2014).
- [30] R. Fei and L. Yang, *Nano Lett.* **14**, 2884 (2014).
- [31] Result of Quantum Monte Carlo calculations (Luke Shulenburger, private communication).
- [32] L. Shulenburger and T. R. Mattsson, *Phys. Rev. B* **88**, 245117 (2013).
- [33] N. Gonzalez Szwacki, A. Sadrzadeh, and B. I. Yakobson, *Phys. Rev. Lett.* **98**, 166804 (2007).
- [34] H.-J. Zhai, Y.-F. Zhao, W.-L. Li, Q. Chen, H. Bai, H.-S. Hu, Z. A. Piazza, W.-J. Tian, H.-G. Lu, Y.-B. Wu, Y.-W. Mu, G.-F. Wei, Z.-P. Liu, J. Li, S.-D. Li, and L.-S. Wang, *Nature Chem.* **6**, 727 (2014).